PAPER

Check for updates

Measurement of CO_2 diffusion coefficients in both bulk liquids and carven filling porous media of fractured-vuggy carbonate reservoirs at 50 MPa and 393 K

Zhixing Wang [iD] [ab] and Jirui Hou *[ab]

Diffusion coefficients are necessary to describe the mass transfer and adsorption rate of CO_2 in formation fluids. However, data is scarcely reported for actual reservoir conditions of high pressure and temperature, which are normal in most scenarios of the CO_2-enhanced oil recovery process in China's fractured-vuggy reservoirs and carbon storage process. Accordingly, this work employed the pressure decay method (PD) and relevant mathematical models to determine the CO_2 diffusion coefficient in both liquids and cavern filling porous media at 50 MPa and 393 K. The effects of the type of reservoir fluids, the properties of carven filling porous media, and water saturation on CO_2 diffusion coefficients were investigated. Results in bulk reservoir liquids showed that the CO_2 diffusion coefficient in the oil sample was 4.1243×10^{-8} $m^2\ s^{-1}$, much higher than those in the pure alkane phase, pure water and brine sample from reservoirs. Results of CO_2 diffusion in carven filling porous media saturated with oil demonstrated a significant dependence on properties such as porosity and permeability, and a correlation in the CO_2 diffusion coefficients between the bulk oil phase and cavern filling porous media in the form of touristy was documented. CO_2 diffusion in the fractured cavern porous media was much higher than that without fracture. An increase in water saturation reduced CO_2 diffusion coefficients in the carven filling porous medium studied, herein. Thus, the CO_2 diffusion coefficient is essentially related to the type of liquid and properties of the filling media.

1 Introduciton

Geological storage of CO_2 gas in deep saline aquifers or depleted oil reservoirs is considered an efficient way to reduce the carbon emission. For petroleum industries, oil recovery can be increased by CO_2 injection as a process fluid into a depleted reservoir. The Tahe oilfield has become the largest marine carbonate hydrocarbon reservoir in China with its equivalent oil–gas reserve at the billion-ton level.[1–3] There are huge potentials for CO_2 storage in this Ordovician carbonate reservoir given that fracture networks and cavities are abundant.[4] Recently, gas injection has been applied in this reservoir.[5,6] By injecting gas into the fracture-cavity production unit, gas contacts the formation fluid *via* diffusion, which causes the oil to swell, reduces the oil viscosity, extracts the light component, lowers the interfacial tension (IFT) and suppresses the water

crest.[7–11] Therefore, the volumetric sweeping and displacement efficiency are drastically improved.

The diffusion coefficient is one of the most basic parameters to determine the mixing rate of the injection gas and reservoir liquids.[12–14] A solution of gas in crude oil causes a series of property changes such as reduction in viscosity and volume expansion, which consequently improve the oil mobility and production capability.[15] From the macroscopic point of view of oil stimulation, the gas diffusion process determines the sweeping efficiency, injection optimization and prediction of gas channeling. The gas diffusivity is also a key parameter to study the enhanced oil recovery mechanism in fractured reservoirs.[16,17] Thus, it is of great importance to investigate the gas diffusivity under real reservoir conditions.

Extensive work has been carried out to determine the diffusion coefficients of carbon dioxide in formation liquids under reservoir conditions. For CO_2 diffusivity in saline aquifers, Raad *et al.*[18] studied the CO_2 diffusivity in synthetic and saline aquifer solutions in the temperature range of 303–310 K and pressure range of 5.88–6.265 MPa. Values in an extended temperature range (268–473 K) at pressures up to 45 MPa were obtained by Lu *et al.*[19] and a power-law relationship with temperature was derived. CO_2 diffusion coefficients under similar conditions

[a]*Research Institute of Enhanced Oil Recovery, Unconventional Petroleum Research Institute, China University of Petroleum (Beijing), Beijing, 102249, China. E-mail: zhxwang0315@126.com; Tel: +86 13998768792*

[b]*Key Laboratory for Greenhouse Gas Sequestration and Oil Exploitation in Beijing, Unconventional Petroleum Research Institute, Beijing, 102249, China. E-mail: houjirui@126.com; Tel: +86 13718816146*

were also measured by Cadogan[20] and correlated with the classical Stokes–Einstein equation. For engineering use, Renner[21] introduced an empirical function simply considering the viscosity of solutions and CO_2 to predict the CO_2 diffusion coefficient for in water or brine. For CO_2 diffusivity in hydrocarbon liquids, Schmidt et al.[22] measured the CO_2 diffusion coefficient in heavy oil at temperatures varying from 293 K to 473 K and pressure of up to 5 MPa, where the temperature was the first reported over 373 K. Values in pure alkanes were reported by Wang et al.[23,24] and Cadogan et al.[25] at temperatures between 298.15 and 423.15 K and pressures up to 69 MPa.

Due to confinement and tortuosity, the phase behaviors of CO_2-alkane systems[26] and mass transfer[27] differ from that in the bulk phase, and studies on CO_2 diffusivity in porous media were reported recently. Li and Dong[28,29] calculated the effective CO_2 diffusion coefficient in Berea cores saturated with n-hexadecane and concluded that the values were slightly dependent on the pressure variation from 2.3 to 6.3 MPa. The effects of oil saturation and tortuosity on CO_2 diffusivity in porous media of low permeability were studied by Li et al.,[30] and it was found that the diffusion coefficients were strongly dependent on the oil saturation and permeability of the porous media. Gao et al.[31] correlated the CO_2 diffusion coefficient with the permeability of porous media by tortuosity and found that high tortuosity retards the CO_2 diffusivity by limiting the gas solubility.

However, the previous measurements of diffusion coefficients still need to be further extended. For CO_2 diffusivity in bulk liquids, theoretical models can achieve high accuracy at a wide range of temperatures and pressures for carbon capture and storage (CCS), but the data of CO_2 diffusion coefficients in alkane mixtures and crude oil is still deficient under real reservoir conditions. For example, the pressure in most reported data is below 10 MPa, which is critical for miscible flooding during gas flooding. For CO_2 diffusivity in porous media, the existing data only covers a limited range of temperatures (<373 K) and pressures (<30 MPa), and the effects of properties such as permeability, porosity and tortuosity are briefly reported. The correlation between the bulk oil phase and porous media still lack experimental verification. These problems become more distinct in the case of CO_2 injection under fracture-vuggy reservoirs, where the temperatures and pressures are extremely high, usually over 393 K and above 30 MPa. Besides, these reservoir characteristics are unique due to the complex fracture networks, discrete vugs and caverns partially filled with various sediments, and complicated oil–water contact. Measuring the CO_2 diffusivity experimentally could facilitate mass transfer under these reservoir conditions.

Herein, the CO_2 diffusion process in bulk crude oil and carven filling media saturated with reservoir fluids were studied at the temperature of 393 K and pressure of 50 MPa, corresponding to the common reservoir conditions of the fracture-vuggy carbonate studied. An improved pressure decay (PD) method was introduced to calculate the effective CO_2 diffusion coefficient. The effects of reservoir fluids and carven filling medium properties, fractures and water saturation on the gas diffusion process were investigated. Several insights in the CO_2

EOR mechanisms in fracture-vuggy carbonate reservoirs were facilitated, offering reference in gas injection optimization.

2 Experimental setup and procedures

2.1 Materials

The crude oil sample used in the experiment was collected from Tahe oilfield, China. The oil viscosity and density were 1.42 mPa s and 0.642 g cm^{-3} under reservoir conditions (413 K and 66.15 MPa), respectively. The saturate, aromatic, resin and asphaltene concentrations of the crude oil used in the experiments were tested, which were 67.14 wt%, 22.09 wt%, 7.72 wt% and 3.06 wt%, respectively. The minimum miscible pressure (MMP) of CO_2 with the oil sample at 393 K was determined using the slim tube experiment, and the results are plotted in Fig. 1. The MMP at the experimental temperature is 52.49 MPa. Brine was also collected from the production well in the same reservoir, with a total mineralization of 2.2×10^5 mg L^{-1}, $CaCl_2$ type. The water viscosity and density were 0.4398 mPa s and 1.15 g cm^{-3} at 393 K and 50 MPa, respectively. The properties of the formation liquids were measured in a PVT cell (PVT240/1500FV, Sanchez Technologies). CO_2 was provided by Jingao Gases with a purity of 99.99%.

The carven filling porous media were made of outcrops corresponding to the formation. According to the statical data of cavern filling porous media from the fracture-vuggy reservoir studied, there were three main types of cavern fillings: breccia (porosity ~20%, permeability ~1000 mD), sedimentary rock represented by sandstone (porosity ~15%, permeability ~500 mD), and siltstone cemented by carbonate minerals (porosity ~10%, permeability ~50 mD). The physical properties of the carven filling porous media are listed in Table 1. All six cores were drilled at the same radius of 3.80 cm and similar length of 8.71–8.97 cm. Cores #1–3 had similar porosities (15.54–19.22%) and permeabilities (687.82–783.40 mD), but the oil saturations ranged from 0.00 to 69.97%. These 3 cores were used to investigate the effect of oil saturation on CO_2 diffusivity. Cores #3–5 were used to study the effect of the cavern filling properties on the CO_2 diffusivity. Their initial oil saturations (S_o) were similar (63.92–71.18%), but their porosities and permeabilities (air permeability, K_{air}, and brine permeability, K_{brine}) were different.
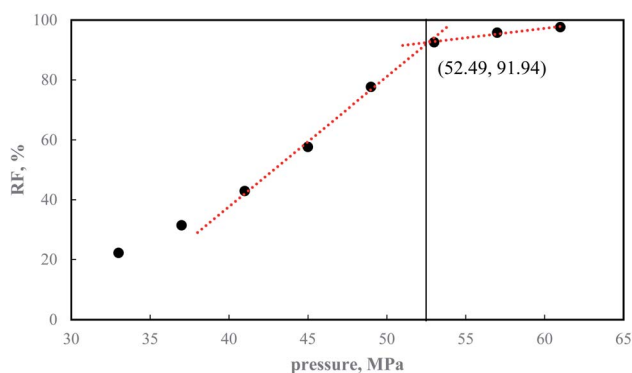

Fig. 1 CO_2 MMP results from slim tube experiment.

Table 1 Properties of carven filling porous media

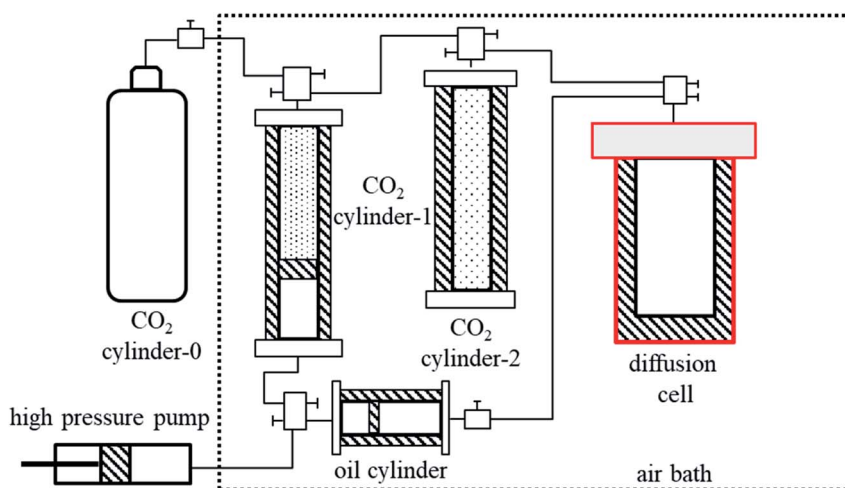| Core no.	Core type	Length (cm)	Radius (cm)	Bulk volume (cm^3)	Pore volume (cm^3)	Porosity (%)	K_{air} (mD)	K_{brine} (mD)	S_o (%)
1	Breccia	8.84	3.802	100.31	16.3	16.25	1292	729	49.69
2	Breccia	8.96	3.802	101.67	15.8	15.54	1389	783	0
3	Breccia	8.71	3.802	98.83	19	19.22	1217	688	69.47
4	Sandstone	8.94	3.802	101.44	17	16.76	83	47	71.18
5	Siltstone	8.97	3.802	101.81	9.7	9.53	10	5	63.92
6	Siltstone	8.76	3.802	99.4	8.1	8.15	8	4	60.49

Fig. 2 Experimental apparatus for the gas diffusion coefficient measurement.

Core #6 was cut in half and used to study the effect of fracture media on CO_2 diffusivity.

2.2 Experimental setup

A schematic diagram of the experimental setup for measuring the CO_2 diffusion coefficients is shown in Fig. 2. It mainly consisted of four components, namely, diffusion cell, gas supply system, data acquisition system, and temperature maintenance system.

A *diffusion cell* with an inner diameter of 5.5 cm and depth of 12.00 cm was used as a holder for the fluids and porous media. The diffusion cell was designed to sustain high pressure of up to 60 MPa and temperature of up to 423 K. The diffusion cell greatly improved the physical limitations of the experimental apparatus[32] and it well covered the experimental condition of 50 MPa and 393 K in this work. As aforementioned, the gas diffusivity in both the bulk liquid and porous media can be studied in the same diffusion cell. Therefore, there are two scenarios in the diffusion cell, as can be seen in Fig. 3. For the gas diffusivity in the bulk liquid phase (scenario #1 in Fig. 3), the diffusion cell was filled with gas (CO_2) and liquid (oil) with an adequate contact interface between the gas and liquid. Scenario #1 was designed to measure the diffusivity without the porous media, representing the condition when CO_2 is injected into caverns without fillings. In the case of the gas diffusivity in porous media, an oil-saturated core was placed inside the

diffusion cell, as can be seen in scenario #2 of Fig. 3. The size of the diffusion cell allowed a relatively large core sample to be placed, and thus there was an enlarged area for gas diffusion into the core through the annular space. Scenario #2 represents the condition when CO_2 is injected to caverns with porous fillings saturated with formation liquids. Consequently, both scenarios covered the conditions when CO_2 is injected to a carbonate reservoir with or without cavern fillings.

2.2.1 Gas supply system. Considering that the operating pressure is normally over 50 MPa, pressurization apparatus was added. As can be seen in Fig. 2, an ISCO high-pressure pump (Model 100DX, Teledyne Technologies) was used for
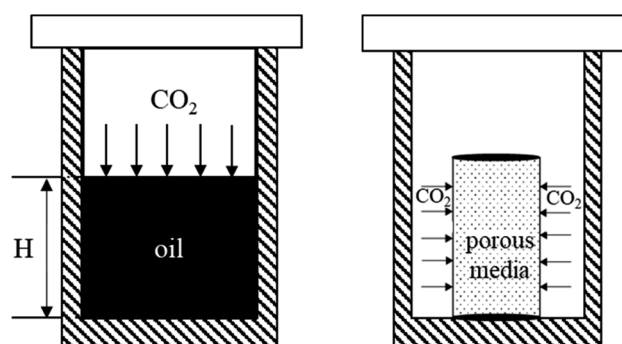

Fig. 3 Gas diffusion scenarios in the diffusion cell (left: scenario #1 and right: scenario #2).

pressurization and precise pressure control. An intermediate container with a piston (CO$_2$ cylinder-1) was used for pressure build-up to achieve a high initial pressure. Considering that the diffusion process begins from the moment CO$_2$ contacts the liquid or porous media, it was necessary to take a shorter time for CO$_2$ to contact the liquid or porous media during the pressure build-up process in the diffusion cell. The instant high pressure in the diffusion cell was offered by an additional gas container (CO$_2$ cylinder-2) instead of the high-pressure ISCO pump. In addition, CO$_2$ cylinder-2 was also set to buffer the turbulent gas flow during the pressurization and diffusion process.

The *data acquisition system* was made of pressure transducers ($\pm$5 kPa accuracy, Model JYB, Collihigh Co., Ltd, China) and computers. The data for the pressure variations with time was monitored and recorded in the computer.

2.2.2 Temperature maintenance system. An air bath ($\pm$0.1 °C accuracy, Model HW-III, Huada Co., Ltd, China) was used to maintain the high temperature for the containers and diffusion cell (dotted lines in Fig. 2).

2.3 Experimental procedures

The pressure decay method has been widely accepted to determine the CO$_2$ diffusion coefficient,[28–31] and thus was applied in this work. The CO$_2$ diffusion coefficient can be calculated by using the recorded real-time pressure data. The designed two scenarios share three main advantages: (1) the procedures are simple and it is easy to transfer liquid or porous media. (2) The improved diffusion flux area either by side surface or liquid surface reduces the sensitivity of the working environment and makes it easy to operate. (3) The pressure distribution in the system is homogeneous during the entire experimental process.

Unlike previous studies, an improvement in the pressure build-up process was made in the experimental procedures. In the previous cases, the pressurization in the diffusion cell was built by directly pumping gas into the oil phase, and the initial pressure was obtained by continuous gas pressurization in the cell. However, the diffusion process took place at the moment when two phases contacted each other, and the pressure may not be accurate in the pressure decay method. In this study, an extra cylinder (CO$_2$ cylinder-2 in Fig. 2) was added between the diffusion cell and the piston cylinder. It was used to generate the initial high pressure instantly in the diffusion cell. By pumping the gas *via* the pump and piston cylinder into cylinder-2, pressure higher than the initial pressure of CO$_2$ was obtained with no contact between the two phases. The procedures for measuring the CO$_2$ diffusion coefficients for the two scenarios are briefly described as follows:

2.3.1 Scenario #1 gas diffusion experiment in the bulk oil phase. (1) Before the diffusion experiment, all the intermediate containers were cleaned using petroleum ether and dried at 373 K in an air bath. A leakage check was performed at 10 MPa using highly purified nitrogen at a temperature of up to 393 K for 2 h.

(2) After CO$_2$ cylinder-1, CO$_2$ cylinder-2, and diffusion cell was vacuumed for 2 h, a desirable amount of oil was injected into the diffusion cell by the ISCO high-pressure pump from the oil cylinder.

(3) CO$_2$ in cylinder-0 was transferred to cylinder-1 and cylinder-2. Then the valve on cylinder-0 was closed and the CO$_2$ in cylinder-1 and cylinder-2 was pressurized by the ISCO pump to a desirable pressure.

(4) The system was maintained at 393 K for 4 h. Cylinder-1 and cylinder-2 were disconnected when the pressure stabilized at a certain pressure (over 50 MPa) prior to the gas diffusion test.

(5) At the beginning of the diffusion test, the pressurized CO$_2$ was transferred from cylinder-2 to the diffusion cell. The real-time pressure in the diffusion cell was recorded by the transducer connected to the computer. The diffusion process be ceased when it reached the steady state.

(6) The CO$_2$ in the diffusion cell was discharged. The liquid in the diffusion cell was removed and all the experimental devices were cleaned for the next measurement.

2.3.2 Scenario #2 gas diffusion experiment in porous media. The procedures for CO$_2$ diffusion in the porous media were similar to scenario #1. However, instead of directly injecting the oil into the cell, a core saturated with the formation fluids was placed in the diffusion cell (see scenario #2 in Fig. 3). The core saturation process was made in an independent core flooding setup, which included a core holder, an ISCO pump, a water cylinder, and an oil cylinder. The core saturation procedures are as follows: (1) the air permeability of the core was measured by a rising bubble apparatus. Also, the bulk volume was acquired by measuring the diameter and length of the core. (2) The core was placed tightly in the core holder with a confining pressure of 10 MPa. It was evacuated for more than 4 h, and then saturated with brine for the pore volume measurement. The brine permeability was measured according to Darcy's law. (3) The core was displaced with the crude oil from the Tahe carbonate reservoir at 0.1 mL min^{-1} until no more water was produced. There are two special cases as follows: for core #1, the water production was half the pore volume to acquire half the oil saturation. For core #2, the oil displacement process was eliminated for 100% water saturation. The oil saturation and irreducible water saturation was then calculated. (4) The liquid-saturated sample was transferred to an air bath together with the core holder. The temperature was set to 393 K for 48 h maturation. (5) The core sample was taken out from the core holder, and both ends of the sample was sealed with the proxy resin.

Once the core was well prepared, it was placed in the center of the diffusion cell (see scenario #2 in Fig. 3). The diffusion test was conducted as follows: the entire system was vacuumed, heated, and pressurized prior to the diffusion experiment similar to that for scenario #1. The pressure data in the diffusion cell was recorded. After the gas-porous media system reached the steady state, the pressure in the diffusion cell was released. The cell was disconnected, opened, and cleaned. A new sample was placed for the next measurement.

3 Mathematical models

As described above, the pressure decay method was used to calculate the CO_2 diffusion coefficient in both scenarios. The mathematical models and solutions are briefly introduced below.

3.1 Gas diffusion experiment in the bulk oil phase

The assumptions made for the mathematical model are as follows: (1) oil evaporation in the CO_2 phase is negligible. The CO_2 gas compressibility factor, Z, is constant. (2) No resistance to mass transfer exists at the CO_2–liquid interface, namely, the concentration at the interface is the equilibrium concentration. (3) The change in the CO_2 diffusion coefficient is not significant during the measurement process. (4) The temperature is constant during the measurement process. (5) Swelling of the liquid by dissolving CO_2 is ignored.

The molar flux of a gas diffusing into a liquid column can be expressed according to Fick's law.[33] It can be simplified to an unsteady-state one-dimensional diffusion in a slab as follows:

$$\frac{\partial C(t,h)}{\partial t} = D_0 \frac{\partial^2 C(t,h)}{\partial h^2} \tag{1}$$

where C is the molar concentration of the gas, mol m^3; h is the diffusion height, m; t is the diffusion time, s; and D_0 is the diffusion coefficient, m^2 s^{-1}.

At the beginning of the diffusion test, the dead crude oil is free of CO_2 and the initial amount of CO_2 is assumed to be zero. The initial condition for eqn (1) can be expressed as:

$$C(t,h) = 0, t = 0, (0 \leq h < H) \tag{2}$$

where H denotes the height of the crude oil, m.

During the diffusion process, the molar concentration at the oil–gas interface varies with pressure and temperature. Considering that the gas diffusion process takes place under isothermal conditions, the CO_2 concentration at equilibrium state, C_{eq}, is solely dependent on the pressure variations.

$$C(t,h) = C_{eq}(P,t), h = H, (0 \leq t) \tag{3}$$

The bottom of the diffusion cell is impermeable. Thus, the rigid boundary condition is applied as follows:

$$\frac{dC}{dh} = 0, h = 0, (0 \leq t) \tag{4}$$

The analytical solution in an infinite series to diffusion eqn (1) subject to the initial condition in eqn (2) and two boundary conditions eqn (3) and (4) is given by Crank:[12]

$$C(h, t) = C_{eq} - \frac{4C_{eq}}{\pi} \sum_{n=0}^{\infty} \left(\frac{(-1)^n}{2n+1} \times \cos\left(\frac{(2n+1)\pi h}{2H} \right) \right. $$
$$\left. \times \exp\left(\frac{(2n+1)^2 \pi^2 D_{AB}}{4H^2} \right) t \right) \tag{5}$$

Combining the gas equation of state (EOS) with eqn (5) above, the pressure *versus* time relation can be derived (gas compressibility factor Z is considered constant due to the small pressure variation during the diffusion process):

$$P(t) - P_{eq} = \frac{8ZRTHC_{eq}}{\pi^2} \sum_{n=0}^{\infty} \left(\frac{1}{(2n+1)^2} \times \exp\left(\right. \right.$$
$$\left. \left. -\frac{(2n+1)^2 \pi^2 D_{AB}}{4H^2} t \right) \right) \tag{6}$$

Neglecting the higher terms over second order of eqn (6), it can be simplified as:

$$P(t) = P_{eq} + a_1 \exp(-b_1 t) + a_2 \exp(-b_2 t) \tag{7}$$

The relation between the measured pressure and time is plotted and then is fit by eqn (7). The diffusion coefficient can be calculated as follows:

$$D_{AB} = \frac{4b_1 H^2}{\pi^2} \tag{8}$$

where H is the liquid height in the diffusion cell, m and D_{AB} is the gas diffusion coefficient, m^2 s^{-1}. The values of a_1, b_1, a_2, b_2 and P_{eq} are determined by non-linear regression of the experimental data. The diffusion coefficient D_{AB} can be calculated using the simple eqn (8) above.

3.2 Gas diffusion experiment in the filling porous media

The assumptions made for the mathematical model are as follows: (1) the cores used in the experiment are homogeneous and isotropic. Fluids are uniformly distributed within the cores. (2) The CO_2 diffusion coefficients in the cores are constant during the measurement process. (3) The CO_2 concentrations in the liquid phase on the core surface are constant during the measurement process. (4) Natural convection caused by the liquid density difference is ignored. (5) Evaporation of the liquid phase into CO_2 is ignored. (6) There is still an interface between CO_2 and the fluids within the porous media.

According to the above-mentioned assumptions, the mathematical description of CO_2 diffusion in porous media can be described as follows:[29,30]

$$\frac{\partial C}{\partial t} = D_{eff} \frac{\partial^2 C(r, t)}{\partial r^2} \tag{9}$$

The initial and boundary condition is:

$$C(r,t) = 0, (t = 0, 0 < r < r_0) \tag{10}$$

$$C(r, t) = 0, (0 \leq t, r = r_0) \tag{11}$$

where $C(r,t)$ and C are the CO_2 concentration during the diffusion process, mol m^3; t is the diffusing time, $t \geq 0$, s; D_{eff} is the effective diffusion coefficient, m^2 s; r_0 is the core radius, m; and r is the CO_2 diffusion radius, $0 < r < r_0$, m.

The analytical solution in an infinite series to diffusion eqn (9) subject to the initial condition boundary condition eqn (10) and (11) is similar to that in eqn (5):

$$C = C_0 \left[1 - \frac{2}{r_0} \sum_{n=1}^{\infty} \frac{J_0(ra_n)\exp(-D_{eff}a_n^2 t)}{a_n J_1(r_0 a_1)} \right] \tag{12}$$
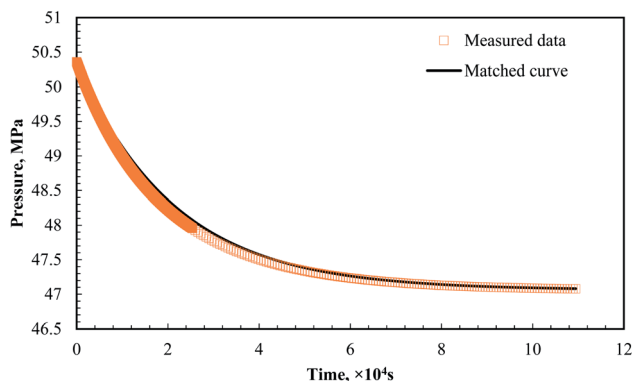
Fig. 4 Measured data VS matched curve using eqn (7) (P_{eq} = 47.06 MPa, a_1 = 1.7153, a_2 = 1.58300, b_1 = 3.9193×10^{-5}, and b_2 = 4.1305×10^{-5}).

Changing eqn (12) in the form of mass and integrating it with r, gives

$$\frac{M_t}{M_\infty} = 1 - \sum_{n=1}^{\infty} \frac{4}{r_0^2 a_0^2} \exp\left(-D_{eff} a_n^2 t\right) \qquad (13)$$

where M_t and M_∞ are the instantaneous and infinite mass of gas dissolved in the porous media, and a_0 and a_n are the positive root of the Bessel function of the first kind.

When $\sqrt{D_{eff} t / r_0^2} < 0.1$, the above equation can be simplified as:

$$\frac{M_t}{M_\infty} \approx \frac{4}{r_0 \sqrt{\pi}} \sqrt{D_{eff} t} \qquad (14)$$

Substituting the real gas EOS $\Delta PV = Z\Delta nRT$ and $M_t = \Delta n$ into eqn (14), eqn (14) can be expressed in the form of the instantaneous pressure difference between the square root of time:

$$\Delta P = \frac{4 M_\infty Z R T \sqrt{D_{eff}}}{r_0 V \sqrt{\pi}} \sqrt{t} = k\sqrt{t} \qquad (15)$$

The mathematical expression of CO_2 diffusion coefficient is determined by eqn (16) through simple linear regression, which has been proven elsewhere.[27,28]

$$D_{eff} = \frac{\pi}{16} \left(\frac{r_0 k V}{M_\infty Z R T}\right)^2 \qquad (16)$$

where r_0 is the radius of the porous media, m; k is the slope of the pressure difference *vs.* the square root of time; V is the CO_2 volume in the annular space between the core and the diffusion cell, m^3; M_∞ is the gas dissolved in the porous media, mole; Z is the CO_2 volume factor, dimensionless; R is the gas constant, and T is the temperature, K.

4 Results and discusion

4.1 CO_2 diffusivity in bulk reservoir liquids

As mentioned above, vugs are the major storage space of formation liquids in fractured-vuggy reservoirs. Herein, for the first time, the CO_2 diffusion coefficient of bulk oil and brine was first studied in the void space under high temperature and pressures.

Fig. 4 shows the pressure data and fit results using eqn (7) for the CO_2–oil system. The CO_2 diffusion coefficient in the oil phase was 4.1243×10^{-8} m² s⁻¹ at 5.10 cm height in the diffusion cell according to eqn (8), and that in heptane was 1.17×10^{-8} m² s⁻¹ under similar conditions according to Cadogen *et al.*[20] The diffusion coefficient of CO_2 in the oil phase was higher than that in liquid heptane. The results presented here may contradict the theoretical Stokes–Einstein models, where the diffusivity of a solute decreases in an alkane with viscosity. This contradiction may be rationalized by considering three typical phenomena from the aspect of the gas enhanced oil recovery process: (1) the CO_2 diffusion coefficient is calculated using the absorption law, where an increase in the difference between the equilibrium solubility and the solute concentration will result in a higher diffusion coefficient being observed. (2) A reduction in viscosity due to CO_2 resolution, a pronounced
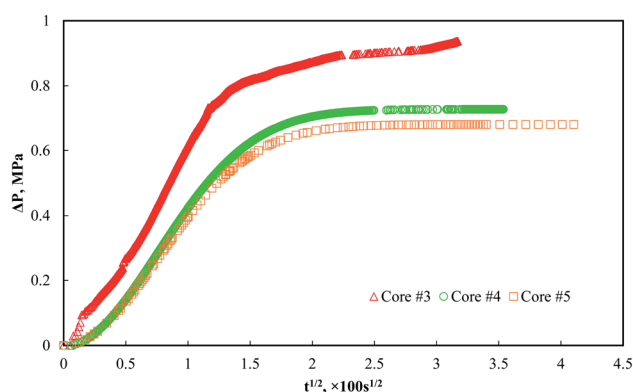

Fig. 5 Pressure difference curves *vs.* time in three different carven filling media.

Table 2 Properties of reservoir fluids and CO_2 under fractured-vuggy reservoirs

Liquid	Temperature (K)	Pressure (MPa)	Density (g cm⁻³)	Viscosity (mPa s)	Diffusion coefficient ($\times 10^{-8}$ m² s⁻¹)
CO_2[a]	393	50	0.7637	0.0680	—
Heptane[a]	398	50	0.6555	0.2729	1.17 (ref. 20)
Oil	403	66	0.6418	1.4200	4.1243
Brine	393	50	1.1500	0.4398	0.2083
Water[a]	393	50	0.9662	0.2448	0.6824 (ref. 35)

[a] Properties of pure components collected from NIST internet database.

Table 3 Pressure drop during CO_2 diffusion in the three filling types

Core no.	Lithology	P_{int} (MPa)	P_{fnl} (MPa)	ΔP (MPa)	$\Delta P/P_{in}$ (%)	CO_2 dissolved ($\times 10^{-5}$ mol)
3	Breccia	50.64	49.70	0.94	1.8511	6.2610
4	Sandstone	50.00	49.28	0.72	1.5779	5.0902
5	Siltstone	50.25	49.58	0.67	1.3536	4.7295

mechanism for gas enhanced oil recovery, decreases the solution (oil phase) viscosity. (3) The oil density increases by the CO_2 solubility in the oil phase, causing an unneglectable natural convection driven by density.

For the CO_2-brine and CO_2-pure water system, the diffusion coefficients in saline aquifer solution and pure water were 0.2083×10^{-8} m^2 s^{-1} and 0.6824×10^{-8} m^2 s^{-1}, respectively (Table 2). The CO_2 diffusivity in brine was lower than that in pure water. According to the statistical analysis by Renner,[21] the diffusion coefficient is highly dependent on both solvent viscosity (water) and solute viscosity (CO_2, in this case), which reflects the influence of temperature, pressure and salinity in water. The addition of salt will not increase the liquid density, where the liquid viscosity will increase,[34,36] which results in a higher resistance for the movement of CO_2 molecules through the water layers. Therefore, the CO_2 diffusivity in the brine decreased compared to that in pure water.

4.2 CO_2 diffusivity in carven-filling porous media with different properties

The vugs within the fractured-vuggy reservoirs are not only filled with liquids but sedimentary rocks due to packing transportation, deposition, and compaction and deformation.[37–39] Over 70% of the void space is partially filled with limestone, sandstone and shale cemented by calcareous material.[40–42] During the gas injection process, the properties of the porous media within the chamber cave are of great importance to analyze the gas sweeping efficiency. Therefore, effect of the cavern fillings properties on the gas diffusion process in fractured-vuggy reservoirs should be investigated. The CO_2 diffusion process in carven fillings saturated with oil was studied in this section.

Fig. 5 plots the pressure difference (delta P, pressure drop compared to the initial pressure, in MPa) vs. the square root of 100 s$^{1/2}$. Unlike the dramatic drop in pressure, the decay curves of CO_2 in the filling media demonstrated a gentle drop as the diffusion continued (Fig. 5). During the initial diffusion stage, the dimensionless pressure variation was irrelevant to the properties of the porous media, all demonstrating a linear decay pattern. CO_2 penetrated the thin oil film first, and then dispersed in the oil in the pores and throats in the porous media. The pressure curves vary in the different porous media as the diffusion proceeded. For siltstone (core #5), with the assumed smallest averaged pore size and the most complicated

Table 4 Properties of cavern fillings of fractured-vuggy reservoirs

Core no.	Lithology	Porosity (%)	Permeability (mD)	Tortuosity[43]	Mean diameter of pore size[43] (μm)	Measured diffusion coefficient ($\times 10^{-9}$ m^2 s^{-1})
3	Breccia	19.22	687.82	3.05	5.34	2.55
4	Sandstone	16.76	46.81	3.42	1.49	1.91
5	Siltstone	9.53	5.23	5.66	0.66	0.69
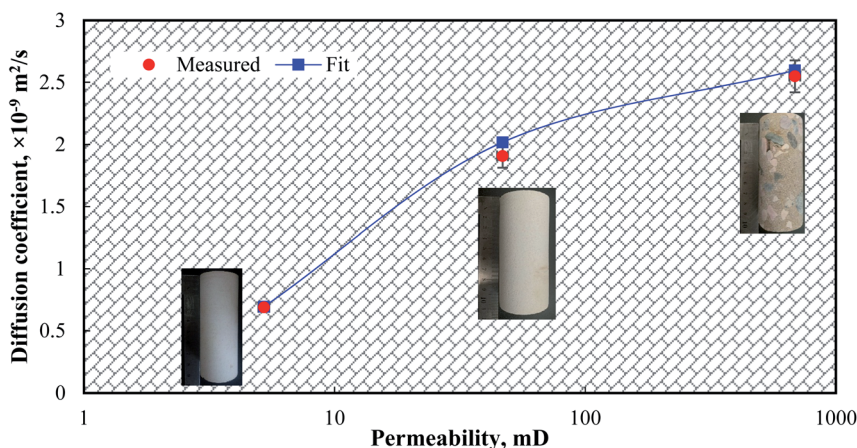
Fig. 6 Comparison of CO_2 diffusion coefficient in three filling patterns of caves.

pore-throat networks (Table 3), the pressure was the last to reach equilibrium and the pressure difference was 0.67 MPa, a 1.35% drop compared to the initial pressure. That in sandstone (core #4) was 0.72 MPa with a 1.58% drop. Also, that in breccias (core #3) was 0.94 MPa with a 1.85% drop. The CO_2 pressure drop in breccia was greater than that in the other two types of cavern filling media, indicating a greater amount of gas was dissolved. The solubility of CO_2 in the cavern filling porous media was calculated according to the equation of state of CO_2 under constant volume condition (Table 4).

The diffusion coefficients obtained using eqn (16) are demonstrated in Fig. 6. The effective diffusion coefficient of CO_2 in breccias (core #3) was 2.55×10^{-9} m^2 s^{-1}, 1.91×10^{-9} m^2 s^{-1} in sandstone (core #4), and 6.89×10^{-10} m^2 s^{-1} in siltstone (core #5) respectively. Due to the complicated sedimentary conditions in carbonate reservoirs, the pores of various diameters are twisted and interconnected with each other, and the path for diffusion of a gas molecule within the pores is "tortuous".[43–45] For CO_2 diffusion in siltstone, which has the highest tortuosity and smallest pore size, it would take the longest time to reach the inside porous media, corresponding to the pressure variations shown in Fig. 5.

In addition, the relationship of CO_2 diffusion between bulk liquid and carven filling media can be described as the effective diffusion coefficient:

$$D_{eff} = \frac{\varphi D_{bulk}}{\tau} \quad (17)$$

where D_{eff} is the gas diffusion coefficients in porous media, D_{bulk} is the gas diffusion coefficient in the bulk phase, and φ and τ represent the porosity and touristy of the carven filling media, respectively. Combing the results in the bulk oil phase and cavern filling media, the measured and fit data using eqn (17) is shown in Fig. 6. The diffusion coefficients of CO_2 measured reflect the relative tortuosity factors under different

permeabilities. As the permeability decreased from 687 mD to 5.23 mD, the tortuosity factor increased by 1.85 times.

Compared to gas diffusion in the void space, the presence of porous media in the vug-cave space lowers the CO_2 mass transfer in these reservoirs. Hence, the gas distribution within the production profile became more heterogeneous, and the property difference in the same production profile enhanced this nonuniformity.

4.3 CO_2 diffusivity in the fractured carven-filling porous media

Besides collapse, breccias and cavern form at any scale, and the associated fracture networks drastically enhance the permeability beyond the matrix. Gas diffusion in the fracture is of great importance for gas injection.[46] During the process of gas injection, CO_2 is injected into the reservoir through the fractures and encompasses the matrix, and the concentration gradient drives CO_2 into the matrix by diffusion. Oil expansion and viscosity reduction occur in the matrix due to the contact of
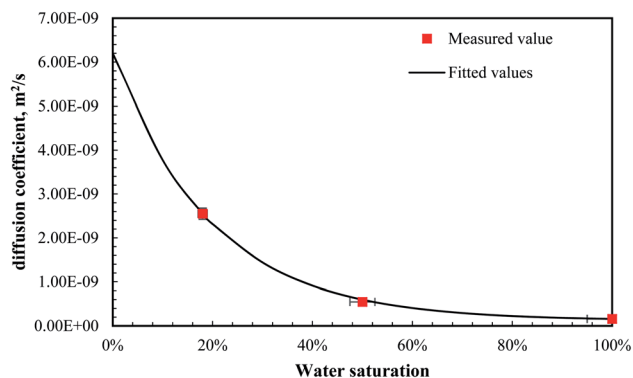

Fig. 8 Diffusion coefficient of CO_2 in breccias saturated with brine water (393 K, 50 MPa, light oil sample, brine).
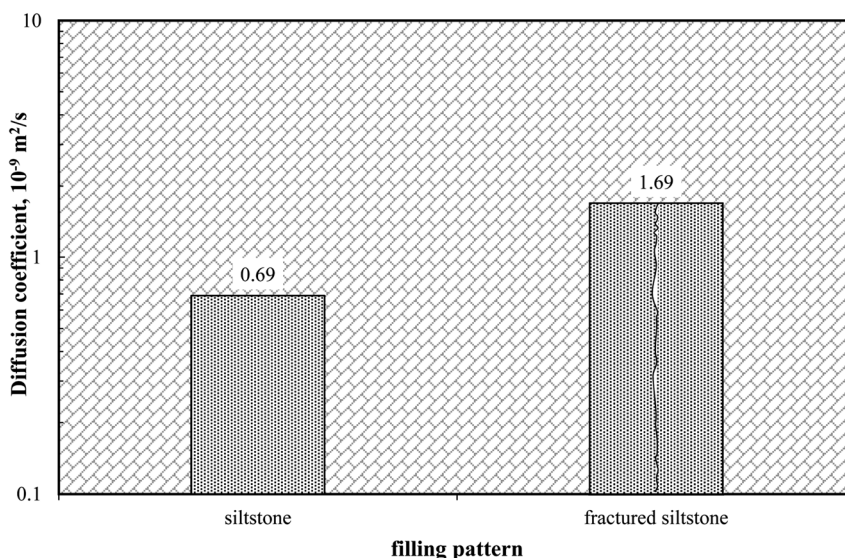

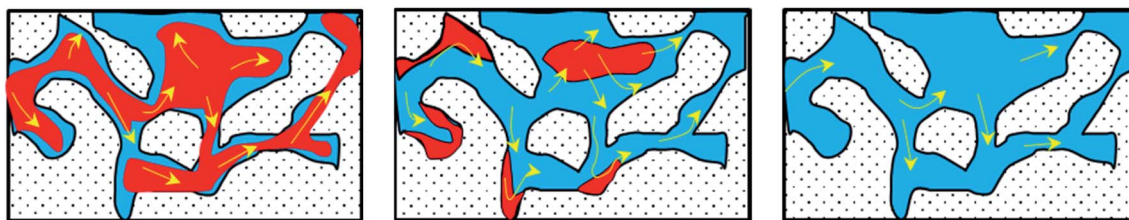**Fig. 7** CO_2 diffusion coefficient in siltstone and fractured siltstone.

Fig. 9 Sketch of CO_2 traces in breccias with various water saturations (left: innate state, middle: $S_w = 50\%$; and right: $S_w = 100\%$).

CO_2. Also, later flow back towards the production well occurs through fracture.[47]

The effective CO_2 diffusion coefficient in both siltstone and fractured siltstone are compared in Fig. 7. As demonstrated below, the CO_2 diffusion coefficient in siltstone was 0.69×10^{-9} m^2 s^{-1}, which increased to 1.69×10^{-9} m^2 s^{-1} in the fractured one, a 2.45-times increase. The existence of fracture significantly improved the gas diffusivity of the cavern siltstone samples. CO_2 flows into the matrix via the fracture surface, enlarging the contact area for gas and matrix. Therefore, mass transfer between separate matrices is enhanced via fractures instead of tortuous pores and throats, allowing more CO_2 to reach inside the porous media.

4.4 CO_2 diffusivity in water-saturated carven-filling porous media

Carbonate materials are susceptible to dissolve in water, and hence splendid river terraces and deep gorges are carved by the subterranean river systems. Karst structures such as subsurface flow channels, solution cavities, sinkholes, pinnacles, and solution chimneys become the flow passages of not only hydrocarbons, but of the water from underground river systems and artificial injection. Production units made up of a single production well or multiple wells suffer excessive water production and reduced production lifetime. Thus, the injection of CO_2 proved to be effective to stabilize oil and water contact, suppressing water cresting in experimental and practical cases. The CO_2 diffusion process at different water saturations is analyzed in this part.

The CO_2 diffusion coefficients in breccias saturated with various water saturations are shown in Fig. 8. The diffusion coefficient decreased from 2.55×10^{-9} m^2 s^{-1} to 1.59×10^{-10} m^2 s^{-1} as the water saturation increased from 18% to 100%. The CO_2 diffusivity declined to 93.76% as the water saturation in breccia increased from initially the connate state to complete saturation in this study.

The measured data was also fit by an exponential decay equation (eqn (18)) and it was found that the CO_2 diffusion coefficient is highly dependent on the water saturation, S_w, within the carven filling porous media.

$$D = 1.21264 \times 10^{-10} + 6.07504 \times 10^{-9} \times \exp(-5.09441 \times S_w) \quad (18)$$

At connate water saturation, most of the oil is a continuous phase between the pore space, while water adheres to the pore body in the form of a film. CO_2 can easily diffuse into pores and

contact with the oil phase, and the diffusion coefficient is relatively high. However, in the water flooded area, a considerable amount of residual oil is isolated from being contacted by the subsequent CO_2 due to water blocking. As listed in Table 2, CO_2 in the oil phase is much higher than that in brine. CO_2 contacts the brine first before dissolving in the oil phase. Considering the existence of torturous pores and throats within the breccia, this transfer process is further delayed. Consequently, the presence of water hinders the CO_2 diffusion process in porous media due to the elevated water saturation (Fig. 9).

5 Conclusion

For a better understanding of the mechanism of CO_2 enhanced oil recovery in the fractured-vuggy carbonate reservoirs in China, the diffusion coefficients were measured using the pressure decay method under reservoir conditions (temperature = 393 K and pressure ≈ 50 MPa). The effects of fluid type, properties of the filling media, and water saturation in the filling media on the CO_2 diffusion coefficients were discussed. The conclusions are as follows:

(1) CO_2 diffusivity in crude oil is almost 8 times higher than that in brine. A huge difference in the CO_2 diffusion coefficients exists between the crude oil and brines under reservoir conditions. Therefore, the mass transfer of CO_2 in the oil phase is more dominant than that in brine, giving priority to the interactions between CO_2 and the oil phase.

(2) The existence of sedimentary rocks in the cavity space hinders the gas diffusion process in saturated oil. The increase in tortuosity in porous media increases the difficulty for CO_2 to transport within fractured-vuggy reservoirs. The rock permeability, pore size, and tortuosity of the pore structures are the key factors that should be considered.

(3) The existence of fractures in sedimentary rock contributes to the CO_2 diffusion process, where the diffusion coefficient increased by over 2 times in this study. Mass transfer is enhanced by the intervened fractures within the carven filling media.

(4) The CO_2 diffusion coefficient shows a significant dependence on the water saturation of the carven filling media. Increasing the brine saturation retards the CO_2 mass transfer in the carven filling media.

Nomenclature

C	Molar concentration of gas, mol m^{-3}
C_{eq}	Molar concentration at equilibrium state, mol m^{-3}

D_0 Diffusion coefficient, $m^2\ s^{-1}$
D_{AB} Gas diffusion coefficient, $m^2\ s^{-1}$
D_{AB} Effective diffusion coefficient, $m^2\ s^{-1}$
h Diffusion distance, m
H Liquid depth, m
k Slope of pressure difference *vs.* the square root of time, MPa $t^{-0.5}$
M_∞ Gas dissolved in the porous media, mol
P Pressure, MPa
R Gas constant, 8.314 J $(mol\ K)^{-1}$
r_0 Core radius, m
r Diffusion radius, $0 < r < r_0$, m
t Diffusion time, s
T Temperature, K
V CO_2 volume in the annular space between the core and the diffusion cell, m^3
Z Gas constant, dimensionless

Conflicts of interest

There are no conflicts to declare.

Acknowledgements

References

1 Y. Li and Z. Fan, Developmental pattern and distribution rule of the fracture-cavity system of Ordovician carbonate reservoirs in the Tahe Oilfield, *Acta Pet. Sin.*, 2011, **32**(1), 101–106.
2 Z. Chen, Y. Dai and Z. Lang, Storage-percolation modes and production performance of the karst reservoirs in Tahe Oilfield, *Petrol. Explor. Dev.*, 2005, **32**(3), 101–105.
3 K. Zhang and D. Wang, Reservoir characterization of the Ordovician oil and gas pools in the Tahe Oilfield, Tarim Basin, Northwest China, *Pet. Explor. Dev.*, 2004, **31**(1), 123–126.
4 J. Allan and S. Sun, Recovery factor in fractured reservoirs: lessons learned from 100 fractured fields, *Pet. Explor. Dev.*, 2003, **30**(6), 129–136.
5 Y. Li, W. Pu, B. Wei, *et al.*, The feasibility of CO_2 and N_2 injection for the Tahe fracture-cavity carbonate extra-heavy oil reservoir: An experimental study, *Fuel*, 2018, **226**, 598–606.
6 X. Lyu, Z. Liu, J. Hou, *et al.*, Mechanism and influencing factors of EOR by N_2 injection in fractured-vuggy carbonate reservoirs, *J. Nat. Gas Sci. Eng*, 2017, **40**, 226–235.
7 Y. Rong, J. Zhao, X. Lu, *et al.*, Remaining oil distribution patterns and potential-tapping countermeasures in carbonate fracture-cavity reservoir, *Acta Pet. Sin.*, 2014, **35**(6), 1138–1146.
8 S. Zheng, M. Yang, Z. Kang, *et al.*, Controlling factors of remaining oil distribution after water flooding and

enhanced oil recovery methods for fracture-cavity reservoirs in Tahe Oilfield, *Petrol. Explor. Dev.*, 2019, **46**(4), 1–9.
9 J. Hui, X. Liu, Y. Wang, *et al.*, Mechanism and Practice of Nitrogen Injection for EOR in Fractured-Vuggy Carbonate Reservoir in Tahe Oilfield, Tarim Basin, *Xinjiang Pet. Geol.*, 2015, **36**(1), 75–77.
10 A. Sharbatian, A. Abedini, Z. Qi, *et al.*, Full Characterization of CO_2–Oil Properties On-Chip: Solubility, Diffusivity, Extraction Pressure, Miscibility, and Contact Angle, *Anal. Chem.*, 2018, **90**(4), 2461–2467.
11 L. Holm and V. Josendal, Mechanisms of oil displacement by carbon dioxide, *J. Pet. Technol.*, 1974, **26**(12), 1427–1438.
12 E. L. Cussler, *Diffusion-Mass transfer in fluid systems*, Cambridge University Press, 3rd edn, 2007, vol. 16, DOI: 10.1017/cbo9780511805134.001.
13 P. Popov, Y. Efendiev and G. Qin, Multiscale. Modeling and simulations of flows in naturally fractured karst reservoirs, *Commun. Comput. Phys*, 2009, **6**(1), 162.
14 L. Rongy, K. Haugen and A. Firoozabadi, Mixing from Fickian diffusion and natural convection in binary non-equilibrium fluid phases, *AIChE J.*, 2012, **58**(5), 1336–1345.
15 M. E. Aguilera and A. López de Ramos, Effect of CO_2 diffusion on wettability for hydrocarbon-water-CO_2 systems in capillaries, *Int. Commun. Heat Mass*, 2004, **31**, 1115–1122.
16 H. Hoteit, Modeling diffusion and gas–oil mass transfer in fractured reservoirs, *J. Pet. Sci. Eng.*, 2013, **105**, 1–17.
17 H. Hoteit and A. Firoozabadi, Numerical modeling of diffusion in fractured media for gas-injection and -recycling schemes, *SPE J.*, 2009, **14**(2), 323–337.
18 J. Raad, R. Azin and S. Osfouri, Measurement of CO_2 diffusivity in synthetic and saline aquifer solutions at reservoir conditions: the role of ion interactions, *Heat Mass Transfer*, 2015, **51**(11), 1587–1595.
19 W. Lu, H. Guo, I. M. Chou, *et al.*, Determination of diffusion coefficients of carbon dioxide in water between 268 and 473K in a high-pressure capillary optical cell with in situ Raman spectroscopic measurements, *Geochim. Cosmochim. Acta*, 2013, **115**, 183–204.
20 S. P. Cadogan, *Diffusion of CO_2 in Fluids Relevant to Carbon Capture, Utilisation and Storage*, Imperial College London, 2015.
21 T. A. Renner, Measurement and Correlation of Diffusion Coefficients for CO_2 and Rich-Gas Applications, *SPE Reservoir Eng.*, 1988, **3**(2), 517–528.
22 T. Schmidt, T. Leshchyshyn and V. Puttagunta Diffusivity of Carbon Dioxide into Athabasca Bitumen, *33rd Annual Technical Meeting of the Petroleum Society of CIM*, 1982, pp. 82−33.
23 L. Wang, Z. Lang and T. Guo, Measurement and Correlation of the Diffusion Coefficients of Carbon Dioxide in Liquid Hydrocarbons under Elevated Pressures, *Fluid Phase Equilib.*, 1996, **117**, 364–372.
24 L. Wang and C. Sun, Diffusion of Carbon Dioxide in Tetradecane, *J. Chem. Eng. Data*, 1997, **42**, 1181–1186.
25 S. P. Cadogan, G. C. Maitland and J. P. Martin, Diffusion coefficients of CO_2 and N_2 in water at temperatures

between 298.15 K and 423.15 K at pressures up to 45 MPa, *J. Chem. Eng. Data*, 2014, **59**, 519–525.

26 G. Yang, Z. Fan and X. Li, Determination of Confined Fluid Phase Behavior Using Extended Peng-Robinson Equation of State, *Chem. Eng. J.*, 2019, **378**, 122032.

27 D. Chai, Z. Fan and X. Li, Gas Transport in Shale Matrix Coupling Multilayer Adsorption and Pore Confinement Effect, *Chem. Eng. J.*, 2019, **370**, 1534–1549.

28 Z. Li, M. Dong and E. Shirif, Transient natural convection induced by gas diffusion in liquid-saturated vertical porous columns, *Ind. Eng. Chem. Res.*, 2006, **45**, 3311–3319.

29 Z. Li and M. Dong, Experimental study of carbon dioxide diffusion in oil-saturated porous media under reservoir conditions, *Ind. Eng. Chem. Res.*, 2009, **48**, 9307–9317.

30 S. Li, Z. Li and Q. Dong, Diffusion coefficients of supercritical CO_2 in oil-saturated cores under low permeability reservoir conditions, *J. CO_2 Util.*, 2016, **14**, 47–60.

31 H. Gao, B. Zhang, L. Fan, *et al.*, Study on Diffusivity of CO_2 in Oil-Saturated Porous Media under High Pressure and Temperature, *Energy Fuels*, 2019, **33**(11), 11364–11372.

32 M. Chordia and J. T. Japan, Diffusion in Naturally Fractured Reservoirs – A Review, Paper presented at the, *SPE Asia Pacific Oil and Gas Conference and Exhibition*, Brisbane, Queensland, Australia, October 2010.

33 Y. Zhang, C. Hyndman and B. B. Maini, Measurement of gas diffusivity in heavy oils, *J. Pet. Sci. Eng.*, 2000, **25**(1), 37–47.

34 J. Crank, *The Mathematics of Diffusion*, Clarendon Press, 2nd edn, Oxford, 1975.

35 R. Azin and M. Mahmoudy, Measurement and modeling of CO_2 diffusion coefficient in saline aquifer at reservoir conditions, *Central Eur. J. Eng.*, 2013, **3**(4), 585–594.

36 W. Zhang, S. Wu, S. Ren, L. Zhang, *et al.*, The modeling and experimental studies on the diffusion coefficient of CO_2 in saline water, *J. CO_2 Utilization*, 2015, **11**, 49–53.

37 C. Mao, J. Zhong, Y. Li, *et al.*, Ordovician carbonate rock matrix fractured-porous reservoirs in Tahe Oilfield, *Pet. Explor. Dev.*, 2014, **41**(6), 681–689.

38 A. Sakhaee-Pour and H. Tran, The Permeability of a representative carbonate volume with a large vug, *Transp. Porous Media*, 2017, **120**, 515–534.

39 P. Baud, U. Exner, M. Lommatzsch, *et al.*, Mechanical behavior, failure mode, and transport properties in a porous carbonate, *J. Geophys. Res.: Solid Earth*, 2017, **122**, 7363–7387.

40 Q. Jin, F. Tian, X. Lu, *et al.*, Characteristics of collapse breccias in caves of runoff zone in the Ordovician karst in Tahe oilfield, Tarim Basin, *Oil Gas Geol.*, 2015, **36**(5), 729–735+755.

41 Q. Jin, X. Kang and F. Tian, Genesis of chemical fillings in fracture-caves in paleo-karst runoff zone in Ordovician and their distributions in Tahe oilfield, Tarim Basin, *Acta Pet. Sin.*, 2015, **36**(7), 791–798+836.

42 Y. Li and Z. Fan, Developmental pattern and distribution rule of the fracture-cavity system of Ordovician carbonate reservoirs in the Tahe Oilfield, *Acta Pet. Sin.*, 2011, **32**(1), 101–106.

43 L. Zhang, J. Ba, L. Fu, *et al.*, Estimation of pore microstructure by using the static and dynamic moduli, *Int. J. Rock Mech. Min. Sci.*, 2019, **113**, 24–30.

44 B. Yu, J. Li, Z. Li, *et al.*, Permeabilities of unsaturated fractal porous media, *Int. J. Multiphase Flow*, 2003, **29**, 1625–1642.

45 J. Wu, D. Hu, J. Guo, *et al.*, Study on the relationship between tortuosity and permeability in porous media, *Journal of North China Institute and Technology*, 2016, **13**(4), 56–59.

46 B. Jia and J, R. Tsau, Barati. Role of molecular diffusion in heterogeneous, naturally fractured shale reservoirs during CO_2 huff-n-puff, *J. Pet. Sci. Eng.*, 2018, **164**, 31–42.

47 S. B. Hawthorne, L. Jin and B. A. Kurz, *et al.*, Integrating petrographic and petrophysical analyses with CO_2 permeation and oil extraction and recovery in the Bakken tight oil formation, Paper Presented at the, *SPE Unconventional Resources Conference*, Calgary, Alberta, Canada, 15–16 February 2017.